

Facile synthesis of yolk shell $\text{Mn}_2\text{O}_3@\text{Mn}_5\text{O}_8$ as an effective catalyst for peroxymonosulfate activation

Aimal Khan^a, Shuhua Zou^a, Ting Wang^a, Jerosha Ifthikar^a, Ali Jawad^b, Zhuwei Liao^b, Ajmal Shahzad^b,
Audrey Ngambia^a, Zhuqi Chen^{a*}

^a Key laboratory of Material Chemistry for Energy Conversion and Storage, Ministry of Education; Hubei Key laboratory of Material Chemistry and Service Failure, School of Chemistry and Chemical Engineering, Huazhong University of Science and Technology, Wuhan 430074, PR China;

^b School of Environmental Science and Engineering, Huazhong University of Science and Technology, Wuhan 430074, PR China,

* Corresponding author:

E-mail address: zqchen@hust.edu.cn (Zhuqi Chen);

List of Figures and tables

Table. 1. Amounts of the precursors used for calcination process and the percentage yield of the catalysts

Table. 2. Show Mn^{2+} ion (ppm) and absorbance values

Fig. S1. XRD pattern of Co_3O_4 and CuO

Fig. S2. TGA profiles of (a) ϵ - MnO_2 , (b) Mn_2O_3 and (c) Mn_3O_4 in air at a heating rate of 10 °C/min.

Fig. S3. SEM images of the as-prepared Mn based materials: (a) ϵ - MnO_2 , (b-f) $Mn_2O_3@Mn_5O_8$

Fig. S4. The efficiency of 4-CP mineralization by $Mn_2O_3@Mn_5O_8$ /PMS system

Fig. S5. Effect of temperature and First order kinetic model of $Mn_2O_3@Mn_5O_8$ catalytic 4-CP reactions.

Fig. S6. Effect of PMS concentration on 4-CP removal. Reaction conditions: Catalyst 0.3 g/L, 4-CP 80 ppm, and temperature: 25 °C.

Fig. S7. Mn ion leaching of $Mn_2O_3@Mn_5O_8$ at different initial pH after 60 min catalytic reaction.

Fig. S8. 4-CP degradation of by homogeneous and heterogeneous catalysis. Reaction condition: Catalyst 0.3 g/L, PMS, 1.5 mM, 4-CP 80 ppm, and temperature: 25 °C.

Fig. S9. Removal of various pollutants on $Mn_2O_3@Mn_5O_8$. Reaction conditions: Catalyst 0.3 g/L, PMS 1.5 mM, contaminants (4-CP, 2, 4,-DCP, Phenol = 80 ppm 2, 4, 6-TCP =10 ppm) and temperature: 25 °C.

Fig. S10. EPR spectra of $^1\text{O}_2$ using TMP. Reaction conditions: Catalyst 0.3 g/L, PMS 1.5 mM, 4-CP 80 ppm, TMP 1.16 g/L, and 25 °C

Fig. S11. (a) XPS wide scan survey before reaction of $\text{Mn}_2\text{O}_3@\text{Mn}_5\text{O}_8$ catalyst; (b) XPS wide scan survey after reaction of $\text{Mn}_2\text{O}_3@\text{Mn}_5\text{O}_8$ catalyst

Text S1.

Chemicals

Mn(CO)₃ (≥ 99%), Co(NO₃)₂·6H₂O (≥ 99%), Cu(NO₃)₂·4H₂O (≥ 99%), NaHCO₃ (≥ 99.5%), NaCl (≥99%), NaNO₃ (≥ 99%), NaH₂PO₄ (≥ 99%), NaClO₄ (≥ 99%), NaOH (≥ 99.8%), MnSO₄·H₂O (≥ 99%), Nitric acid (65~68%), 1,4-benzoquinone (98.7%), Phosphoric acid, chlorophenols (4-CP, 2,4-DCP, 2,4,6-TCP), phenol, tert-Butanol, methanol and other chemicals were purchased from Sinopharm Chemical Reagent Co., Ltd (Shanghai, China). 2,2,6,6-tetramethyl-4-piperidinol (TMP, 99%) and sodium azide (NaN₃) were purchased from Sigma-Aldrich, Iron oxide (II, III) (>99.5%) and Potassium periodate were purchased from Aladdin industrial corporation. Oxone (2KHSO₅·KHSO₄·K₂SO₄) and 5, 5-dimethyl-1-pyrrolene-N-oxide (DMPO) (98%) were purchased from Adamas Reagent Co., Ltd and was used as received without further purification.

Text S2.

2.3 Characterizations

X-ray diffraction (XRD) equipped with diffractometer of Cu K- α radiation ($\lambda=1.540598$ Å) (PAN alytical B.V. EMPYREAN) was used to analyze the crystallinity of catalysts in powder form. The morphology of the catalyst was characterized by a high resolution field emission (FEI Nova Nano SEM 450) and a high resolution transmission electron microscopy (TEM) Tecnai G20 American. The surface area and pore size distribution was analyzed by micromeritics ASAP 2420 USA. FTIR was obtained in the range of 400-4000 cm⁻¹ by Fourier transforms infrared (FTIR) spectrophotometer with KBr as the reference transmittance (Bruker vertex 70 American). Thermogravimetric analysis (TGA) was used for phase change and thermal stability of catalysts by a TGA6

PerkinElmer with a rising temperature rate of 10 °C min⁻¹ from room temperature to 1000 °C. X-ray photoelectron spectra (XPS) on Kratos Axis Ultra spectrometer ELD (Kratos Corporation) with monochromic Al K α radiation as the exciting source (225 W) was used for the analysis of composition and oxidation states. Binding energies were calibrated versus the carbon signal at 285 eV.

Thermodynamic tests

First order kinetic model (equation 1) was used for the curve fitting of oxidative degradation, whereas k was the first order rate constant, C was the detected concentration after certain reaction time (t), and C₀ was the initial concentration.

$$\ln\left(\frac{C}{C_0}\right) = -kt \quad (1)$$

Kinetic rate constants of 4-CP degradation by Mn₂O₃@Mn₅O₈ were measured separately under different temperatures of 25, 35 and 45 °C, respectively. The correlation between constants and temperatures was fitted by the Arrhenius relationship, based on which the activation energy was calculated.

Text Detail of EPR studies

Electron paramagnetic resonance (EPR) spectrometry studies was conducted as follows: a solution of 0.3 g/L catalyst, 1.5 mM PMS, 4-CP 80 ppm and different spin-trapping reagent was mixed and analyzed by EPR spectrometer (JEOL FA200, Japan) at room temperature. Conditions: sweep width: 100 G; microwave frequency: 9.87 GHz; modulation frequency: 100 GHz; and power: 18.11 mW.

Text. 3. Detail of analysis manganese ions (Mn^{2+} and Mn^{4+}) in reaction solution via UV-Vis spectroscopy

The leached sample was analysed by ICP for sample, 5.6 mg/L was detected at lower pH =3.6. Moreover, both Mn^{2+} and Mn^{4+} in reaction solution were investigated by UV-Vis spectroscopy. First, the stock solution of manganese ions (100 ppm Mn) was prepared from $MnSO_4$. The deionized water was used for solutions manganese ions (Mn^{2+}), and was an almost colourless solution. For manganese ions, acid (H_3PO_4 =5 mL) was used for easily oxidized to permanganate ions, Potassium periodate, KIO_4 (0.4 g) was used to oxidize $Mn^{2+}(aq)$ to the purple $MnO_4^-(aq)$ ion. Small quantities of manganese can be determined as highly coloured permanganate ion, which exhibits a maximum absorbance at 525 nm. Then, UV-Vis spectroscopy was used for all standards solutions as well as for leached Mn ions sample. Various concentration of Mn^{2+} ions and leached Mn ions Solution were prepared and diluted to 50 mL. The absorbance values mentioned in table. S2. It should be noted that 15 mL leached sample of Mn ions was also diluted to 50 mL. Then plotted standard solution ppm vs absorbance values as shown in table.S2

$$y = mx + c$$

$$0.32423 = \text{slope} * \text{Conc} + \text{intercept}$$

$$\text{Conc} = \frac{0.32423 - (\text{intercept})}{\text{Slope}}$$

$$\text{Conc} = \frac{0.32423 - (-0.00219)}{0.06957}$$

$$\text{Conc} = 4.69 \text{ ppm}$$

$$\text{Total leaching} = 5.6 \text{ ppm}$$

Thus, from above calculation, we got concentration for Mn^{2+} (4.69 ppm) and others for Mn^{4+} (0.91 ppm).

Table. S1. Amounts of the precursors used for calcination process and the percentage yield of the catalysts

Catalysts	Amount of precursors MnCO-100	Amount of catalysts after calcination	Percentage yield of catalysts
ϵ -MnO ₂	5.045 g	4.315 g	85.46%
Mn ₂ O ₃ @Mn ₅ O ₈	5.027 g	3.541 g	70.43%
Mn ₂ O ₃	5.008 g	3.379 g	67.47%
Mn ₃ O ₄	5.005 g	3.233 g	64.59%

Table. S2. Show Mn²⁺ ion (ppm) and absorbance values

S.No	Mn (ppm)	Absorbance
1	1	0.070619
2	2	0.130324
3	3	0.208135
4	4	0.268715
5	5	0.352542
6 (sample)		0.097272, $(0.097272 \times 3.33 = 0.32423)$

Fig. S1

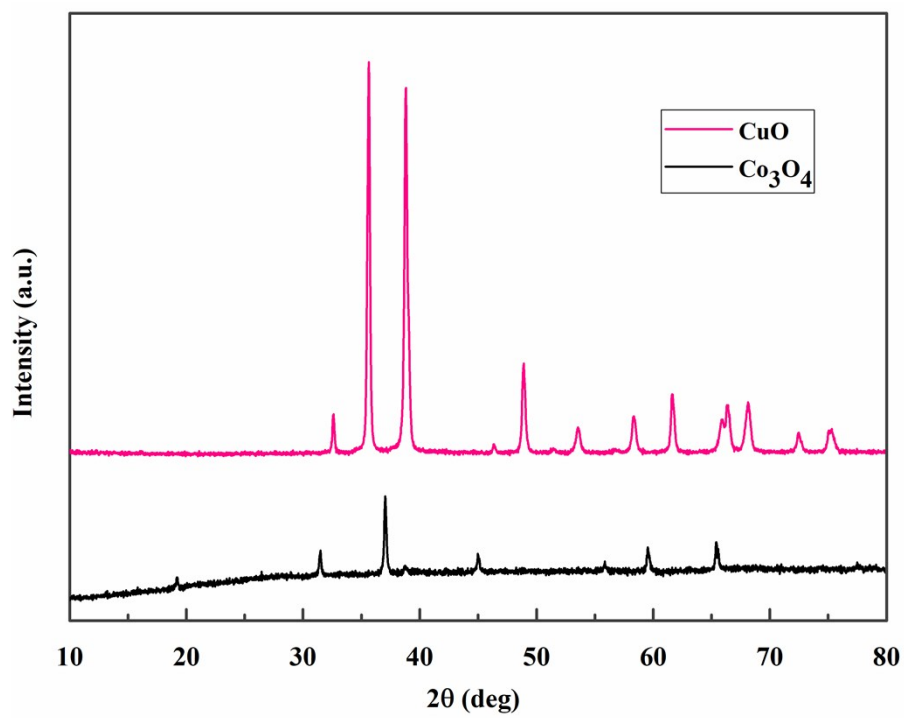


Fig. S1. XRD pattern of Co_3O_4 and CuO

Fig. S2

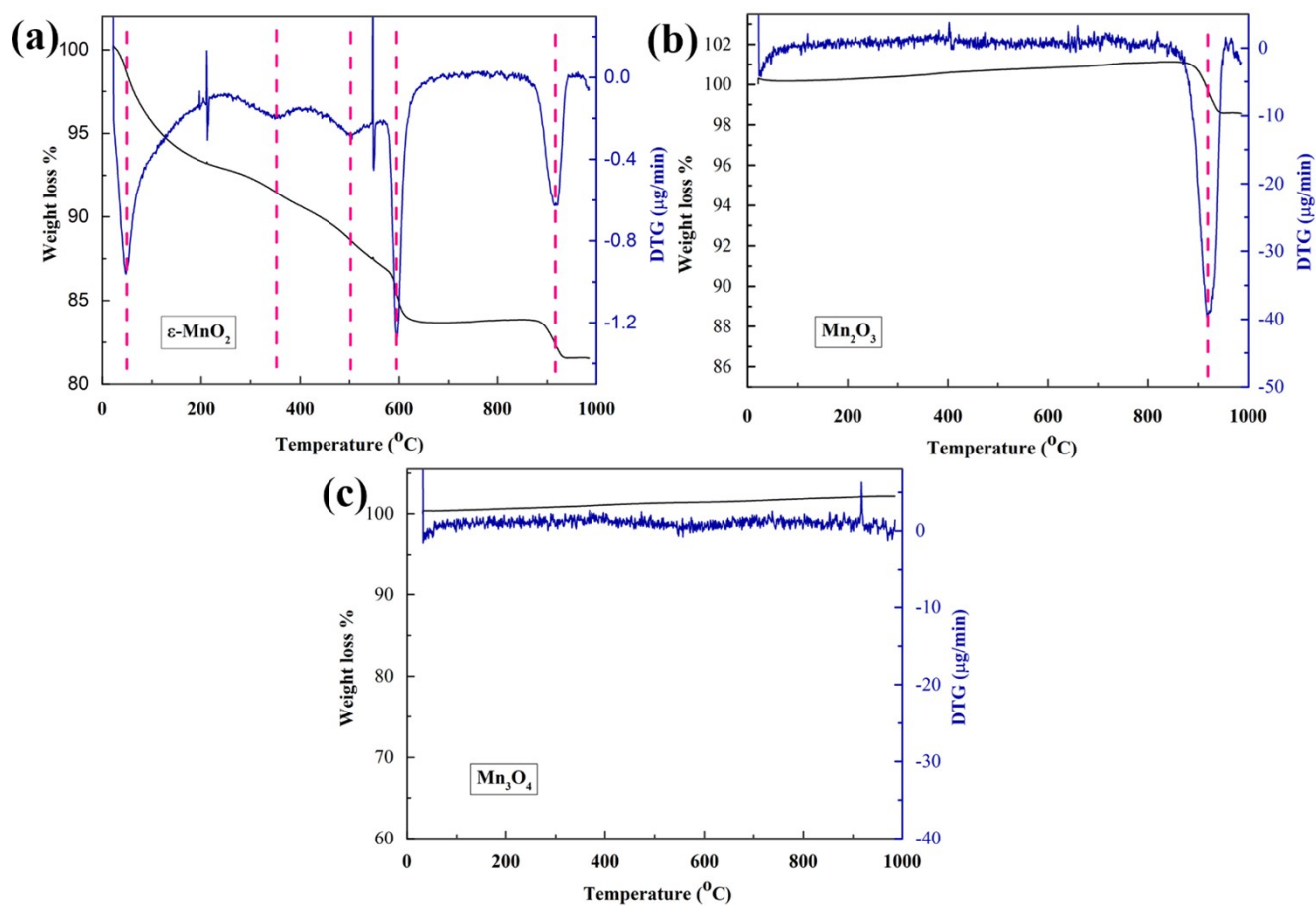


Fig. S2 TGA profiles of (a) $\epsilon\text{-MnO}_2$, (b) Mn_2O_3 and (c) Mn_3O_4 in air at a heating rate of $10^{\circ}\text{C}/\text{min}$.

Fig. S3

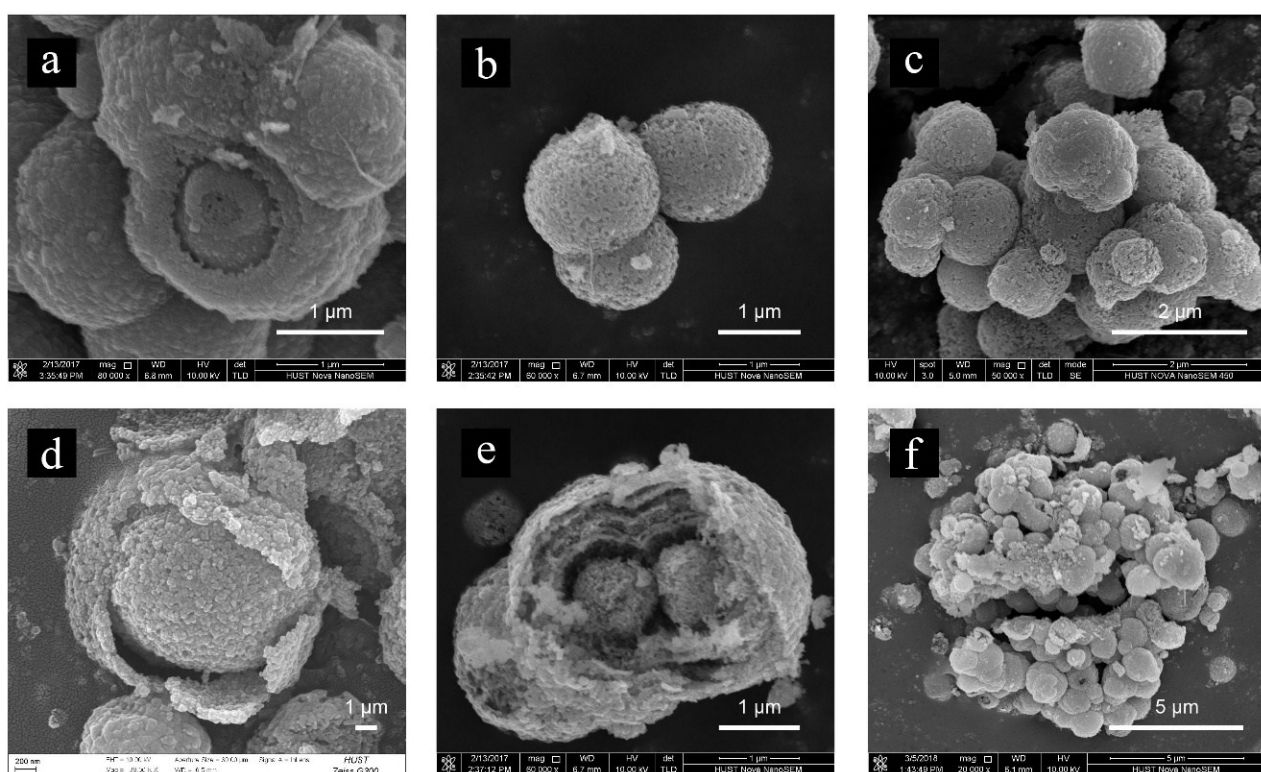


Fig. 3. SEM images of the as-prepared Mn based materials: (a) ϵ - MnO_2 , (b-f) $\text{Mn}_2\text{O}_3@\text{Mn}_5\text{O}_8$

Fig. S4

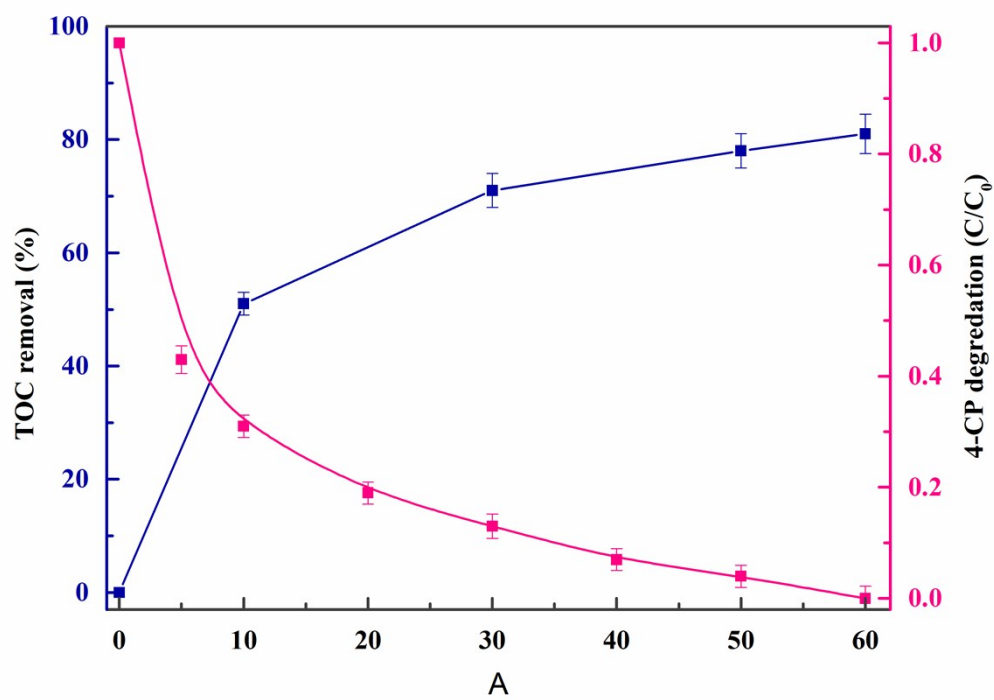


Fig. S4. The efficiency of 4-CP mineralization by $\text{Mn}_2\text{O}_3@\text{Mn}_5\text{O}_8/\text{PMS}$ system

Fig. S5

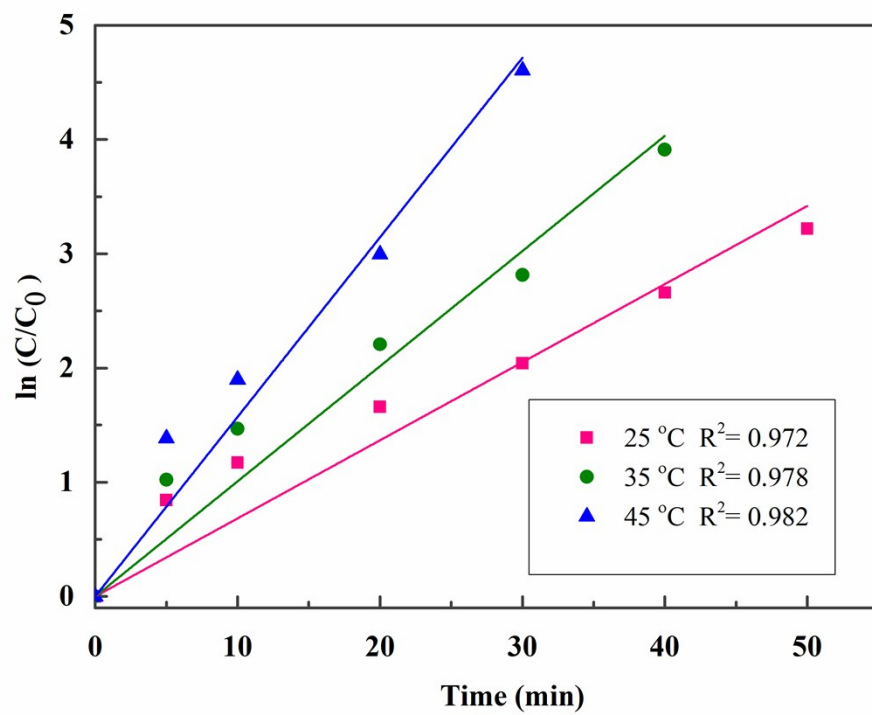


Fig. S5. Effect of temperature and First order kinetic model of $Mn_2O_3@Mn_5O_8$ catalytic 4-CP reactions.

Fig. S6

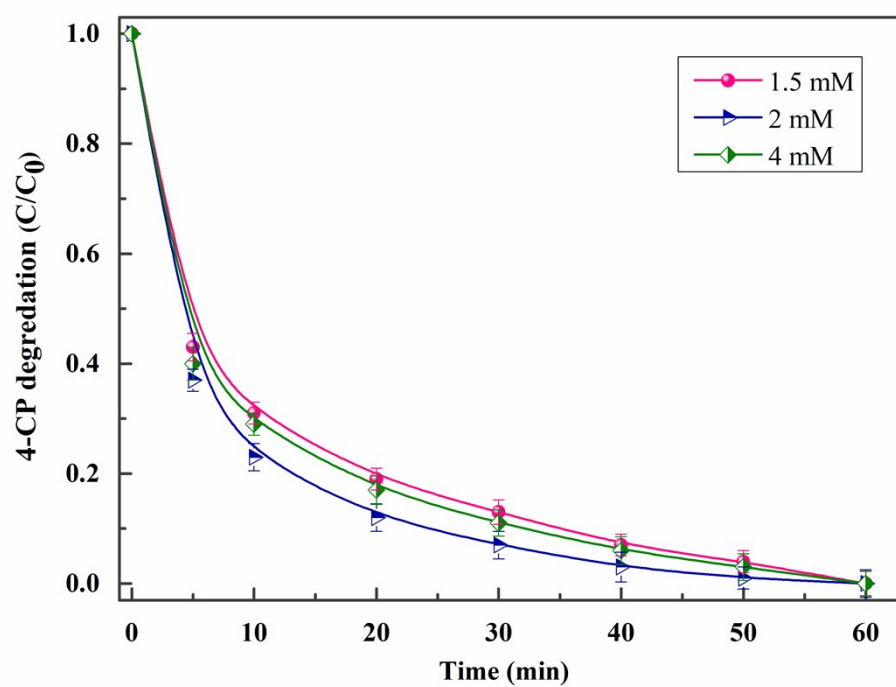


Fig. S6. Effect of PMS concentration on 4-CP removal. Reaction conditions: Catalyst 0.3 g/L, 4-CP 80 ppm, and temperature: 25 °C.

Fig. S7

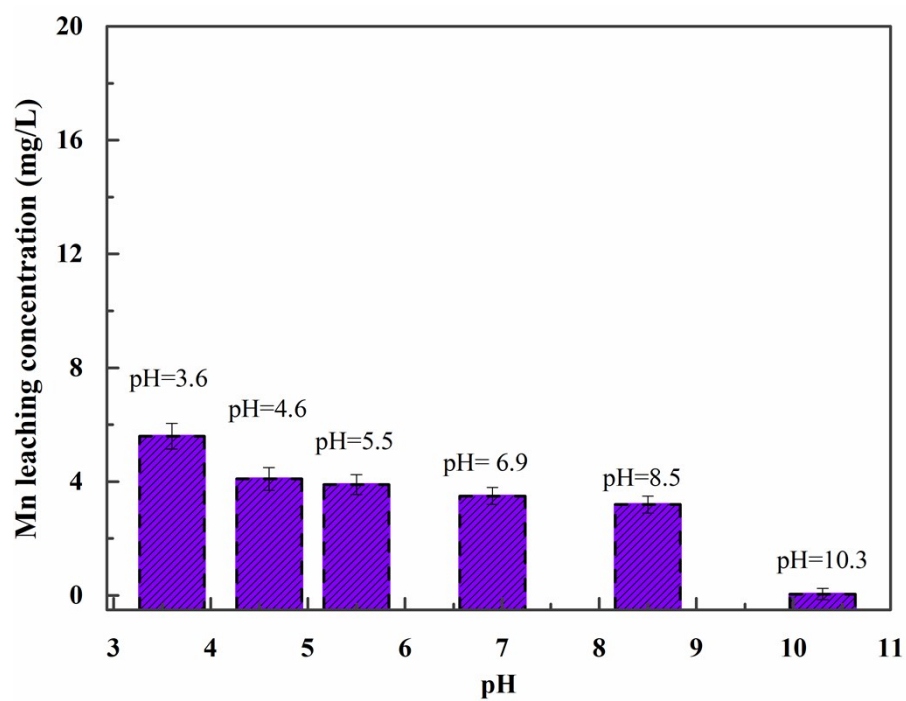


Fig. S7. Mn ion leaching of $\text{Mn}_2\text{O}_3@\text{Mn}_5\text{O}_8$ at different initial pH after 60 min catalytic reaction. Reaction condition: Catalyst 0.3 g/L, PMS, 1.5 mM, 4-CP 80 ppm, and temperature: 25 °C.

Fig. S8

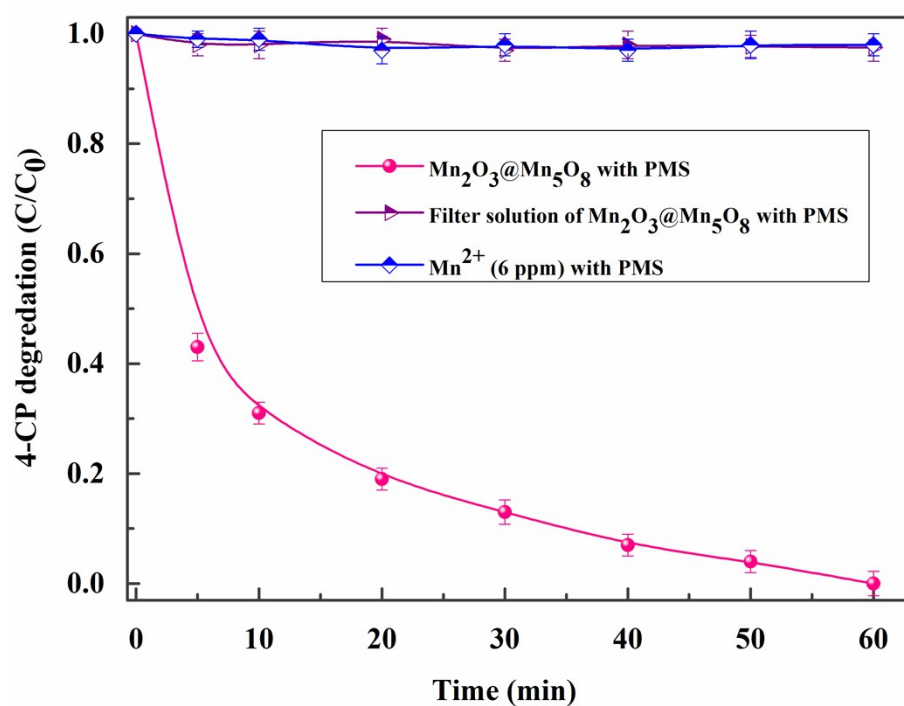


Fig. S8. 4-CP degradation of by homogeneous and heterogeneous catalysis. Reaction condition: Catalyst 0.3 g/L, PMS, 1.5 mM, 4-CP 80 ppm, and temperature: 25 °C.

Fig. S9

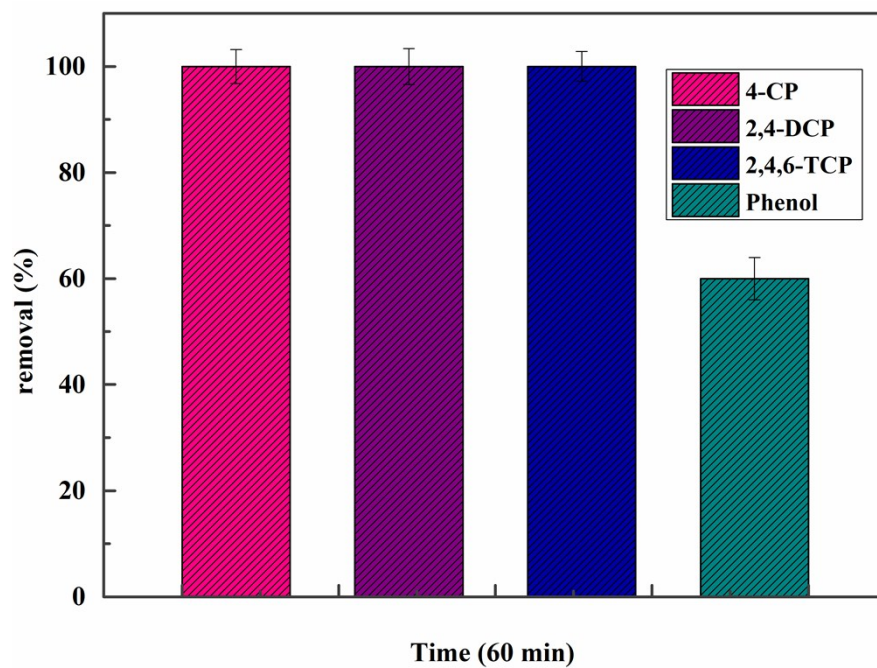


Fig. S9. Removal of various pollutants on $\text{Mn}_2\text{O}_3@\text{Mn}_5\text{O}_8$. Reaction conditions: Catalyst 0.3 g/L, PMS 1.5 mM, contaminants (4-CP, 2, 4,-DCP, Phenol = 80 ppm 2, 4, 6-TCP =10 ppm) and temperature: 25 °C.

Fig. S10

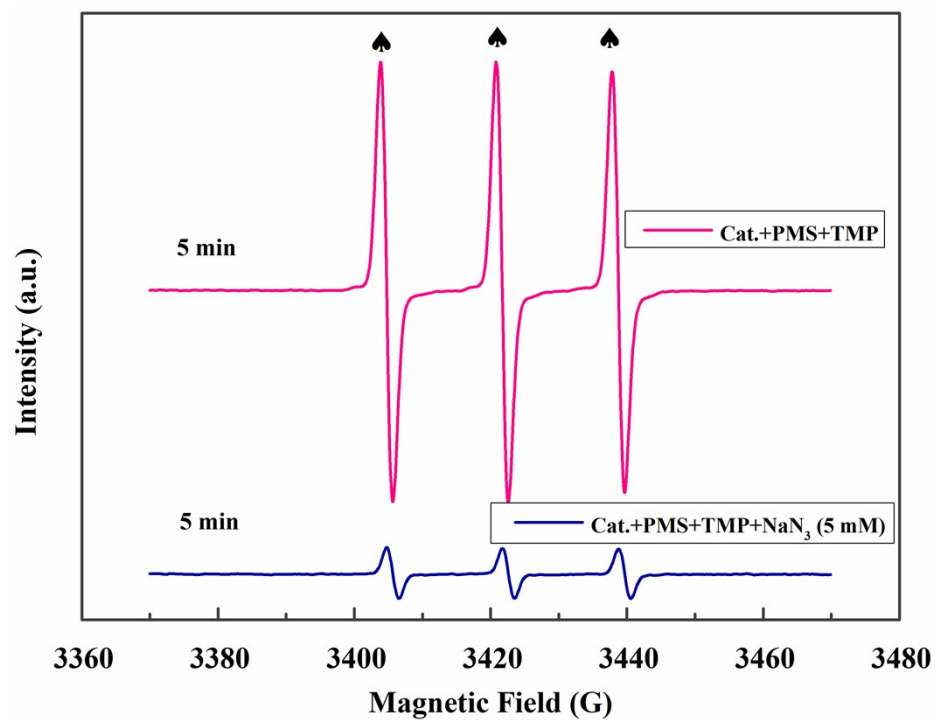


Fig. S10. EPR spectra of $^1\text{O}_2$ using TMP. Reaction conditions: Catalyst 0.3 g/L, PMS 1.5 mM, 4-CP 80 ppm, TMP 1.16 g/L, and 25 °C

Fig. S11

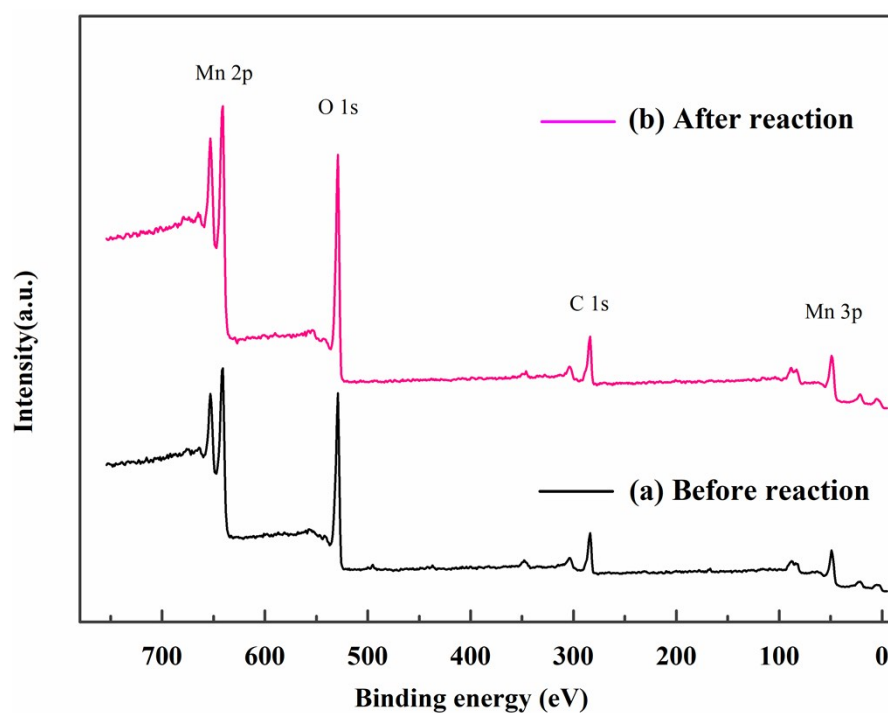


Fig. S11. (a) XPS wide scan survey before reaction of $\text{Mn}_2\text{O}_3@\text{Mn}_5\text{O}_8$ catalyst; (b) XPS wide scan survey after reaction of $\text{Mn}_2\text{O}_3@\text{Mn}_5\text{O}_8$ catalyst